



A Linear Inchworm Piezomotor with a New Configuration: Design Considerations, Fabrication and Characterization

Mohammad Sangchap^{1,2} · Mohammad Tahmasebipour^{1,2,3} · Younes Tahmasebipour²

Received: 23 December 2019 / Accepted: 28 October 2020 / Published online: 16 November 2020
© Shiraz University 2020

Abstract

The new technologies of precise positioning systems with high speed and accuracy have been in the focus of attention in the recent years. In this research, a one-axis walker type inchworm piezomotor has been designed, modeled, manufactured and characterized. Simple design, simple manufacturing and assembly processes, low manufacturing cost and also high speed and stroke are advantages of this piezomotor. This system consists of three piezoelectric actuators, which installed into the clamps and feeder sets, and a guideway. The geometrical parameters with a high impact on the stiffness have been realized and modeled by the finite element method to ensure the proper functioning of the piezomotor. The motor dimensions are $55 \times 23.1 \times 15 \text{ mm}^3$ which can provide a large movement range inside the guideway. The simulation analysis and experimental tests have been carried out to characterize the piezomotor. Based on the shape mode analysis, the maximum operating frequency of the piezomotor has been determined. Also, the Von-Mises stress analysis has been employed to predict the structural behavior of the motor. Finally, the experimental tests have been conducted to illustrate the piezomotor characteristics such as step pitch, speed, and operating frequency.

Keywords Precision positioning system · Inchworm piezomotor · One-axis piezomotor · Piezoelectric motor · Piezoelectric actuator

1 Introduction

In the recent years, nanopositioning systems and piezoelectric motors have been utilized extensively in some technological applications such as semiconductor devices manufacturing apparatus, biological sample manipulation, scanning probe microscopes (SPMs), optical instruments, alignment automation, and robotics. With the invention of the atomic force microscope and the scanning tunneling microscope, some significant advances have been made in the medical, chemical, material and physics sciences. One

of the most widely used applications of the precise positioning systems is the scanning of the sample surface and control the interaction between the surface and the probe of the atomic force microscope. Since then, the scanning probe microscopes have been considered as a valuable tool to study and manipulate the objects (Tahmasebipour et al. 2009; Tahmasebipour et al. 2010; Fleming and Leang 2014; Ru et al. 2016). Precision positioning systems are used to move the objects within the nanometric resolution and with a high speed (from micrometer to millimeter per second) in a limited range. Due to the superior advantages of the piezoelectric actuators, the majority of the nanopositioning systems utilizes the piezoelectric elements to obtain an accurate long stroke. Therefore, piezoelectric actuators due to their advantages such as quick response, extreme fine strain, large force creation, lightness, and high precision play a vital role in the nanopositioning systems. However, their slight range of movement and hysteresis phenomenon are some drawbacks for these actuators, but some solutions have been presented to overcome these issues. The first problem is solvable by employing the frequency leveraging approach, which is a way to create high displacements by integrating

✉ Mohammad Tahmasebipour
tahmasebipour@ut.ac.ir

¹ Faculty of New Sciences and Technologies, University of Tehran, Tehran, Iran

² Micro/Nano-Fabrication Technologies Laboratory, Faculty of New Sciences and Technologies, University of Tehran, Tehran, Iran

³ Micro/Nanofluidic Systems Laboratory, Faculty of New Sciences and Technologies, University of Tehran, Tehran, Iran

small displacements resulted from frequency stimulation. The hysteresis effect also can be compensated by the proper selection of a well-designed closed-loop controller (Cao and Chen 2015; Powers et al. 2003).

The nanopositioning systems have been categorized into two groups of linear and rotary motors. The motion principles in these systems are classified into resonant and non-resonant mechanisms. The Ultrasonic motors, which placed in the first category, is used to work close to the structure's resonant frequency. On the other hand, the non-resonant systems work far from the resonant modes and include different motion principles such as flexure-guided actuators, inertial motors, and inchworm piezomotors (Spanner 2006; Shafik and Mrad 2016; Peng et al. 2015; Yong et al. 2012). Flexure-guided mechanisms because of the stroke limitation, which is constrained to the piezoelectric strain, the inertial motors because of the rollback, accuracy loss and small bearing capacity, and ultrasonic motors because of the high power consumption, complexity in design, and complicated driving circuit are not a good candidate for designing the long range high resolution piezomotors. On the other hand, the inchworm mechanism has some advantages like providing a high range of the movement, low manufacturing cost and low power consumption, which distinguish it from other actuation types. This mechanism offers two different working principles named as walker types and pusher types. In the walker type, the piezomotor is placed into a guideway and can displace by interacting with it. A beam (shaft) can be moved by associating with the piezomotor, in the pusher type. A literature review related to the inchworm piezomotors has been presented in the following paragraph.

The first generations of the inchworm piezomotors had a simple rigid structure, and sometimes required at least two driving actuators to establish a desired motion (Galutva et al. 1972). Fujimoto manufactured a one-axis walker piezomotor which comprises of four piezoelectric actuators. Two of the actuators were used for driving the feeder set, and two other ones for driving the clamp set. In addition to the high manufacturing cost, due to the utilization of the flexure-guided arms, this system suffered from a low stiffness. Thus, the low flexibility of the structure led to the small bearing capacity (Fujimoto 1988). Jian-Tian Pan et al. created a once-axis walker piezomotor. The axisymmetric configuration of the clamp sets and micrometer resolution are some of the flaws for this research (Pan et al. 2000). Gao et al. designed a two DoF system, which utilized the inchworm mechanism. The experimental results include 10, 20 nm resolution and 40, 45 μm movement range in each axis, respectively. The limited area of the operation is a weakness for this design (Gao et al. 2000).

Galente et al. developed a pusher type piezomotor with the dimensions of 60*40*20 mm³ and specifications such as 6 mm range of movement, a few tens of micrometers

resolution, maximum speed of 6 mm/s and load bearing capacity of 40 N. Clamp and feeder actuators of this system fed with an electrical voltage with amplitude of 124 V, 0–87 V, respectively (Galente et al. 1999). Roberts et al. created a walker type piezomotor with a cylindrical configuration that operated along the z-axis. The motor specifications were 4.4 mm/min speed, 22 N load bearing, and 25 mm stroke (Roberts 1999). Tenzer et al. fabricated a one-axis piezomotor prototype with load bearing capacity of 150 N, the supply voltage of 100 V and the maximum speed at the resonance mode and non-resonant mode of 20 mm/s and 8 mm/s, respectively (Tenzer and Mrad 2004). Li et al. utilized a flexure mechanism combined with the inchworm mechanism to amplify the output displacement of the piezoelectric actuators. The features of this piezomotor include resolution of 60 nm, the load-bearing capacity of 11 N, and the maximum speed of 1.259 mm/s and displacement range of 25 mm. By employing the flexure mechanism into the design, it degrades the stiffness of the piezomotor and consequently, makes its functional specifications inappropriate (Ma et al. 2015).

In the present research, a one-axis walker type inchworm piezomotor has been designed, modeled, manufactured and characterized. The finite element analysis (FEA) method has been utilized to realize the impact of the clamp and feeder parameters on their stiffness to achieve a suitable design. FEA also was carried out to realize the resonance modes and Von Mises stresses distribution in the piezomotor structure. Simple design, simple manufacturing and assembly processes, low manufacturing cost and also high resolution, speed and stroke are advantages of this piezomotor.

The operating principles of the proposed one-axis walker type piezomotor is elaborated on Sect. 2.1. In Sect. 2.2, the fundamental design principles of the motor is presented. In the following, the effect of the clamp and feeder actuators' geometric parameters on the amount of the stiffness is investigated. Lastly, in Sect. 2.3, we refer to the steps taken to fabricate the piezomotor. In Sect. 3, the simulation and experimental results that carried out to characterize the piezomotor specifications are presented.

2 Materials and Methods

2.1 Operating Principle of the Proposed Piezomotor

In the present research, a one-axis walker type piezomotor has been designed, modeled, manufactured and characterized. Inchworm mechanism is one of the most applicable principles for designing the nanopositioning systems. This mechanism relies on the frequency stimulation to create an integrated step from small displacements. The operating principle of the proposed piezomotor includes a six-stage

mechanism in which stimulation of the piezoelectric actuators will create a periodic step-by-step movement. Figure 1 illustrates the motion principle of this motor. With stimulation of the clamp actuator 1 in step A, this actuator locks to the guideway. The feeder actuator is then excited to move the clamp 2 by one step along the horizontal axis in step B, while the clamp 1 form remains active. In step C, the clamp 2 engages to the guideway while Clamp1 and Feeder actuator are still turned on. By deactivating the clamp actuator 1 in Step D, clamp 1 disengages from the guideway. In Step E, the feeder actuator is turned off and came back to its initial position, but the clamp 2 remains active which results in the movement of clamp 1 to the right by one step. Ultimately in stage F, clamp 2 remains active and clamp1 locks to the guideway. By repeating this six-step cycle, a continuous movement is obtained along the one-axis. The excitation signals to driving the piezomotor in each step are shown in the Fig. 2. All of the driving signals have distinctive phase shifts with the following settings: Phase difference of 60 degrees between the Clamp 1 and the feeder, and phase shift of 120 degrees between the Clamp 1 and Clamp 2.

2.2 Clamp and Feeder Actuators Design Considerations

The configuration of the proposed one-axis inchworm piezomotor has been demonstrated in Fig. 3. This structure comprises two clamps and one feeder actuator which responsible for creating a step-by-step movement inside the guideway. The clamp structures are identical and attached to the feeder structure. Three piezoelectric actuators are placed inside the clamp and feeder structures. Geometrical dimensions of the designed piezomotor have been given in the Table 1.

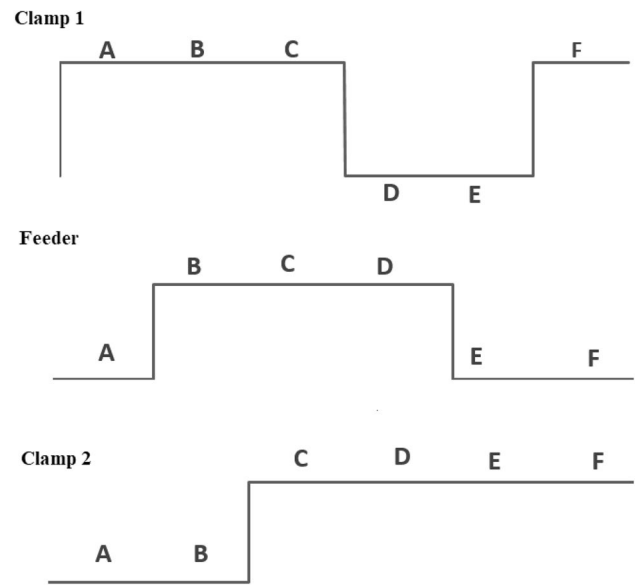


Fig. 2 Driving signals sequence of the clamps and feeder actuators

One of the critical considerations of designing the piezomotor systems is the amount of clamp and feeder stiffness. Since this parameter plays a pivotal role for proper operation, the geometrical parameters which have a substantial impact on the stiffness need to be selected appropriately. Another important consideration is material selection. Since the piezoelectric actuator yields a significant force, a considerable amount of stress might be an issue for this system. Thus, the material that utilized in this research is Stainless Steel 420. This material was hardened with the heat treatment process for having excellent characteristics such as high resistance and stiffness. The mechanical attributes of heat treated stainless steel are shown in Table 2.

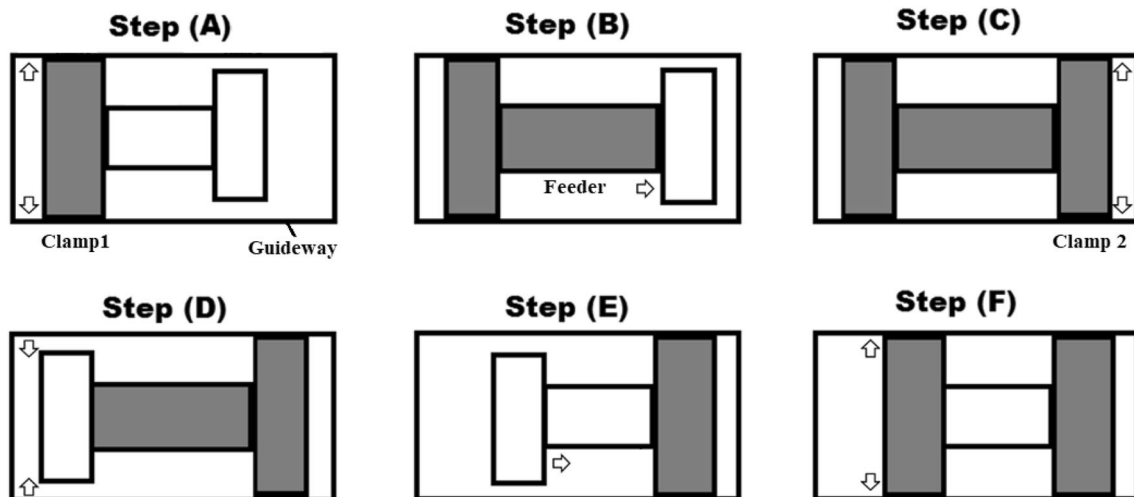


Fig. 1 Operating principle of the proposed walker type inchworm piezomotor

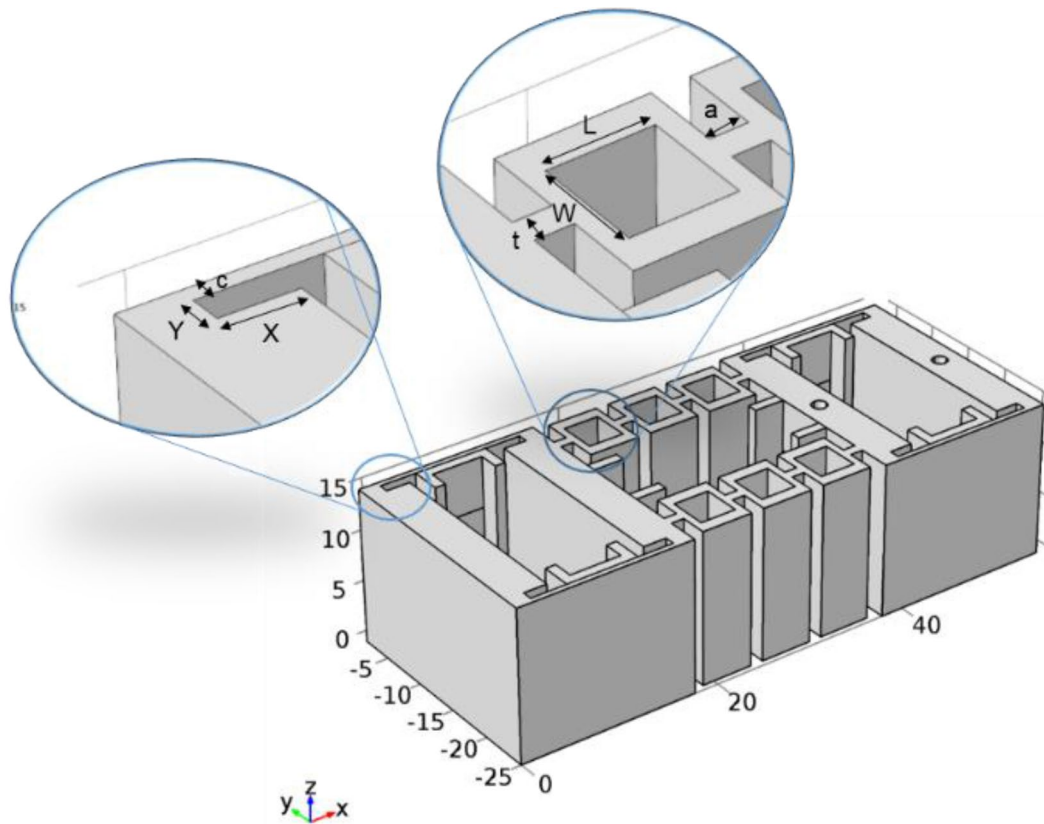


Fig. 3 One-axis walker type piezomotor

Table 1 Geometrical dimensions of the one-axis walker type piezomotor

	Length (mm)	Width (mm)	Thickness (mm)
Piezomotor Dimensions	55	23.1	15
Clamp Structure	17.5	23.1	15
Feeder Structure	20	23.1	15

Table 2 Mechanical characteristics of the Stainless Steel 420

Material Type	Density (kg/m ³)	Young Modulus (Gpa)	Yield Stress (MPa)	Poisson's Ratio
420SS	7800	200	1700	0.28

The clamp sets of this piezomotor need to specific mechanical attributes to engage/disengage to the guideway appropriately. Similarly, the feeder set which defines the piezomotor step size needs to have an optimized stiffness to work rightly. Using the Finite Element Analysis (FEA)

method, the effects of the geometrical parameters shown in the Fig. 3 on the axial stiffness are computed. The proper stiffness for the clamp sets should be determined low, because of flexibility is essential for the clamp set to engage/disengage with the rail. The feeder stiffness should be high due to its required high stability to deal with a wide range of temperature (Vijaya 2016). As a result, the required stiffness for the clamps and feeder sets are determined to be in the range of 10–20 N/ μ m and 40–50 N/ μ m, respectively (Zhang and Zhu 1997; Zhang et al. 1997; Tenzer and Mrad 2004).

The geometrical parameters with a considerable impression on the stiffness of the piezomotor named as: clamp thickness (c), groove length (X) and groove width (Y) for the clamp sets, and interface structure length and width between the spring cavities (a and t), and length and width of the spring cavities (L and W) for the feeder set. The range of these parameters are given in the Table 3. The direct effect of each parameter, while the other parameters remain constant, have been studied on the stiffness; First we found out the suitable value for each geometrical parameters, then we put them fixed during our simulations to their designated values and studied the effect of the other parameter. For example to understand the effect

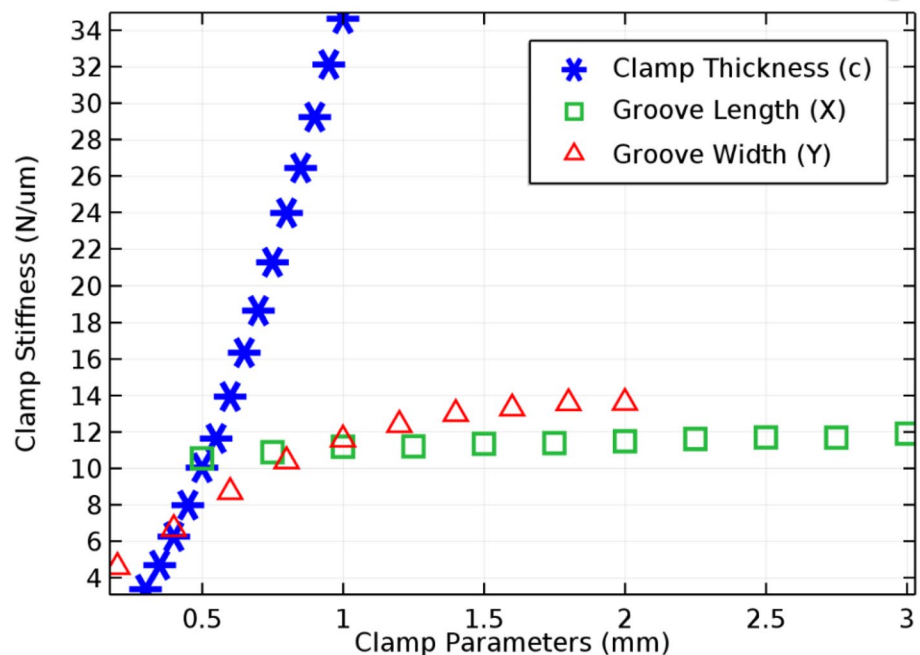
Table 3 Geometrical parameters range of the piezomotor

Parameters	Least value (mm)	Maximum value (mm)	Pitch (mm)
c	0.3	1	0.05
X	0.5	3	0.25
Y	0.2	2	0.2
a	0.25	1.5	0.25
t	0.25	2.5	0.25
L	2.75	4.25	0.5
W	3	4.5	0.5

of the clamp thickness (c) on the stiffness we put all other parameters constant on their suitable values ($X = 2.25$ mm, $Y = 1$ mm, $a = 1.25$ mm, $t = 1$ mm, $W = 3.75$ mm, $L = 4$ mm).

Figure 4 describes the effect of the clamp set's geometrical parameters, which defined as the clamp thickness (c), groove length (X), and groove width (Y), on the stiffness. As previously discussed, the desired amount of the clamp stiffness is in the range of 10–20 N/ μ m. As is apparent in the Fig. 4, with increasing the clamp thickness, the stiffness grows rapidly. The least stiffness corresponds to the clamp thickness of 0.3 mm is 3.21 N/ μ m, while the maximum value of the stiffness corresponds to the 1 mm clamp thickness is 34.65 N/ μ m. Based on the determined stiffness criteria, the best selection range for the clamp thickness is 0.5–0.7 mm, which on this paper is chosen as 0.55 mm that related to the 11.65 N/ μ m stiffness.

Fig. 4 Clamp set stiffness versus the clamp geometric parameters



Additionally, the clamping stiffness for all values of groove length (X) is in the designated range (10.6–11.9 N/ μ m). However, it should be noted that the different values of the groove length affect the deflection amount of the interface structure between the feeder and the locking clamp set, which can lead to the undesired reduction of the step pitch of the piezomotor, that will be discussed in the following. The stiffness of the clamp also slightly increases with rise of the groove width (Y). The appropriate selection range for Y is from 0.8 to 2 mm, which is selected 1 mm for this design.

A part of the piezostack displacement is not transferred to the released clamp by bending of the interface structures between the feeder and the clamp sets. As mentioned earlier, the clamp groove length affect the deflection of the interface structures. Figure 5 shows the deflection of the interface structures versus the groove length, when the piezomotor is in the feeder mode. The maximum deflection of the interface structures is 9.65 μ m corresponds to the groove length of 0.5 mm and the least value is 1.5 μ m that happens for the 3 mm groove length. The acceptable deflection for the disired operation of the piezomotor is considered less than 3 μ m. Also, it should be noted that the assembling process of the piezoelectric actuators faces some difficulties for the groove length more than 2.25 mm. As a result, the ultimate choice for this parameter must be 2.25 mm which makes the deflection of 2.3 μ m in the interface structure.

Figure 6 shows the effect of variation of the feeder's set geometrical parameters such as length a and width t of the interfaces between springs on the stiffness. As is observed in the figure, with the increase of length "a", the

Fig. 5 Deflection of the interface structures between the feeder and clamp sets for different groove lengths

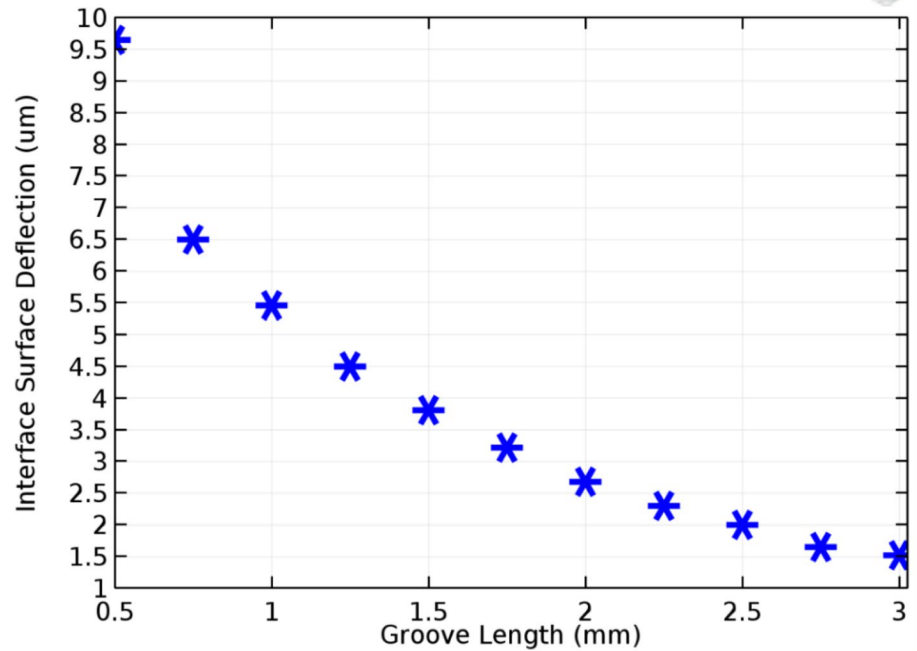
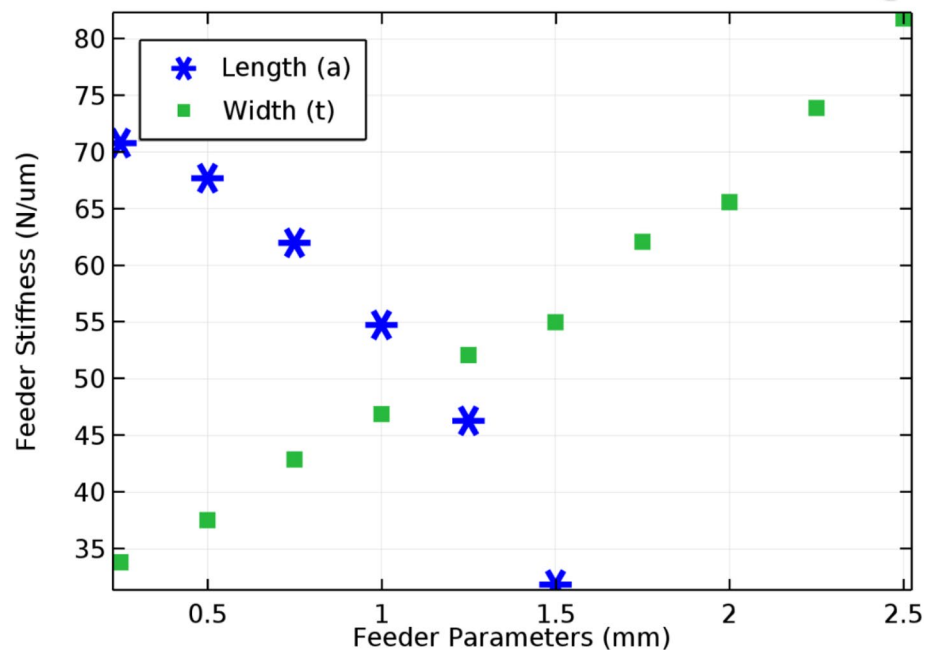


Fig. 6 Feeder stiffness versus the feeder geometrical parameters a and t



feeder stiffness diminishes linearly, and the optimal stiffness (40–50 N/ μ m) can only be achievable for the value of 1.25 mm. so the length “ a ” was considered to be 1.25 mm. Additionally, with the increase of width t , the feeder stiffness increases linearly. The least and most feeder stiffness is 33.82 and 81.08 N/ μ m which occurs for the width t of 0.25 and 2.5 mm, respectively. The acceptable range for

width t is within the range of (0.75–1.25 mm), which was selected 1 mm for this system.

Figure 7 shows the effect of spring cavities area on the feeder stiffness. With the rise of the L and W , the spring hole area increases, which leads to the reduction in the feeder stiffness. The maximum and minimum feeder stiffness are 423.03 and 10.55 N/ μ m corresponds to the cavity area of

Fig. 7 Feeder Stiffness versus the area of spring cavity

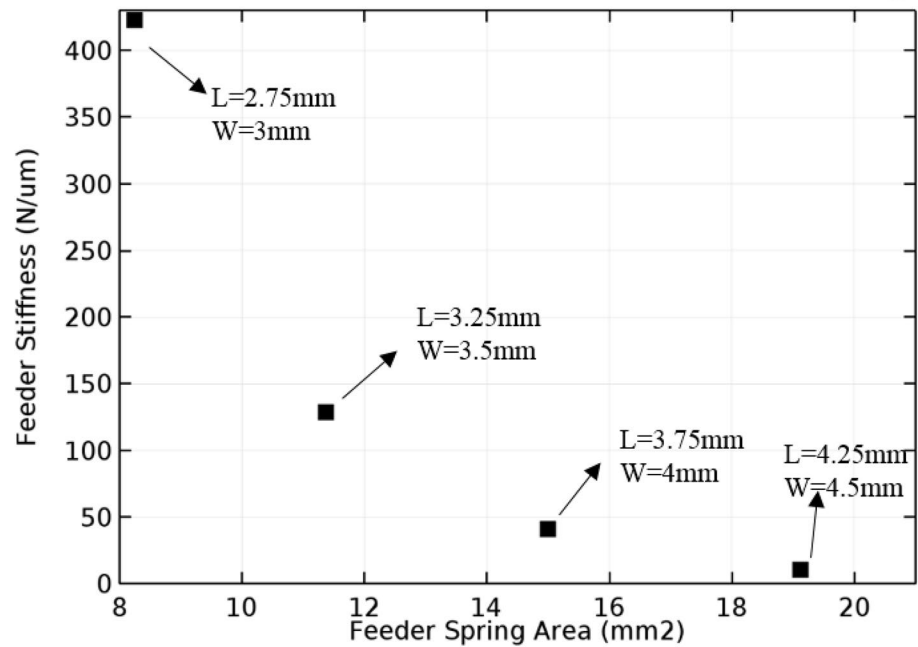


Table 4 The geometrical features of the one-axi piezomotor

Clamp set parameters		Feeder set parameters	
c	0.55 mm	a	1.25 mm
X	2.25 mm	t	1 mm
Y	1 mm	(L,W)	(3.75, 4) mm

8.25 and 19.125 mm², respectively. The spring cavity area is determined as 15 mm², corresponds to the W and L of 3.75 and 4 mm, respectively. In summary, the geometrical features of the clamp and feeder sets is presented in Table 4.

2.3 Manufacturing Process

The manufacturing process of the proposed one-axis piezomotor includes three steps of heat treatment, electric discharge machining (EDM), and surface finishing processes. A significant increase of the mechanical stress might be created on the flexible areas of the piezomotor during the operation. In order to guarantee a safe performance, at first step, the mechanical characteristics of the stainless steel 420 have been improved by the heat treatment approach. This process included three main phases named: hardening, tempering, and quenching processes. Subsequently, the electric discharge machining was performed on the hardened steel to attain the anticipated geometry of the structures. This process can be used for micro-fabrication (Tahmasebipour et al. 2017, 2019) and nano-fabrication

(Tahmasebipour et al. 2011; Tahmasebipour et al. 2014). Finally, the surface finishing process was applied to the fabricated structures.

3 Characterization

In this section, the simulation results such as shape modes and Von-Mises stress analysis are carried out to indicate the maximum operating frequency and to ensure the system safety by using the COMSOL software. The experimental tests like the displacement and speed tests are also implemented to realize the piezomotor's characteristics.

All the three piezostack actuators that were used in the proposed inchworm piezomotor are from the PiezoDrive company with a dimension of 5 × 5 × 20 mm³, natural frequency of 74 kHz and stiffness of 41 N/um. The experimental set-up used to realize the system's attributes is illustrated in Fig. 8. Firstly, the voltage signals, which are generated from the computer by using a homemade LABVIEW-based control program, are transmitted to the driving circuit. In the following step, these signals being converted to the desired ones, which are required to drive the piezomotor in the fine mode and coarse mode, via the electronic circuit and finally transferred to the piezomotor. A digital optical microscope (a product of the DinoLite company) with the magnification factor up to 250 times and a laser displacement meter (Optex CD22) are utilized to measure the displacement of the piezomotor.

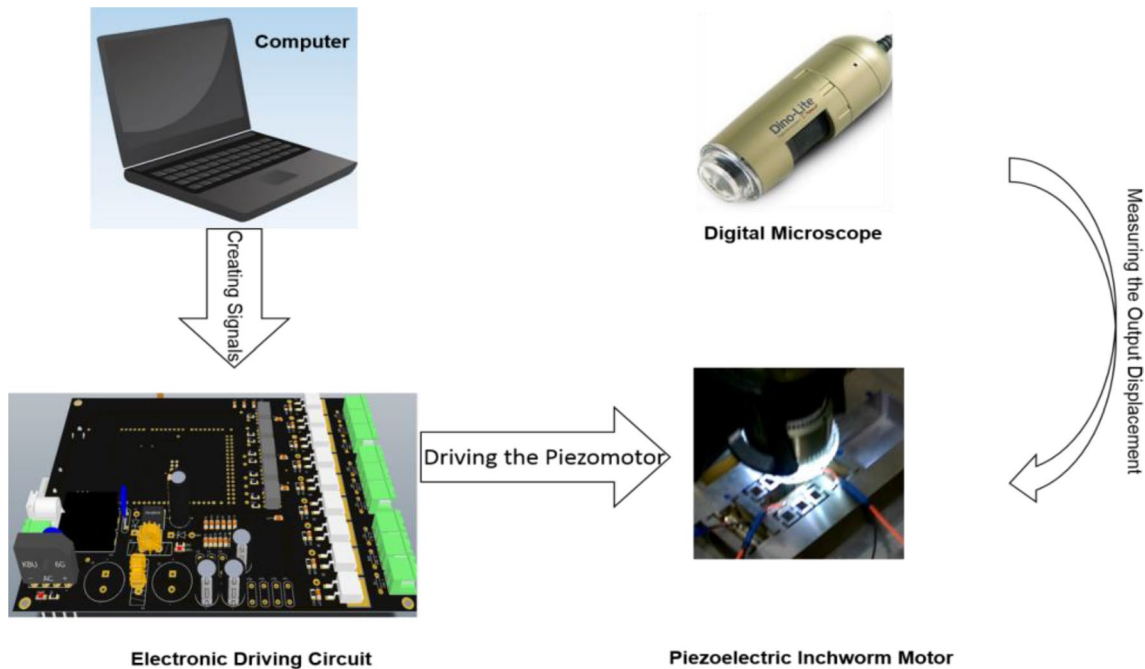


Fig. 8 Experimental Set-up used for characterization of the piezomotor

3.1 Frequency Analysis

The simulation results of the first six shape modes of the piezomotor are shown in Fig. 9. The definitive natural modes for this system are the ones that stimulate the piezomotor in its moving directions. As seen in the figure, the piezomotor oscillates at the clamp and feeder directions in the first and fifth shape modes corresponds to the natural frequencies of 679.97 Hz and 5117.6 Hz, respectively. As a result, the limitation of the operating frequency is determined by the first resonance mode (679.07 Hz).

3.2 Von Mises Stress analysis

The primary objective of the Von Mises stress analysis is to ensure the structural integrity of the system with a reasonable margin of the safety. Due to the presence of a preload that is applied to the piezoelectric stack actuators, the induced Von-Mises stress throughout the system involves both of the preload and the applied load during the piezomotor operation under the maximum applied voltage. Based on the recommendation of the piezostack actuator's manufacturer, the PiezoDrive Corporation, the preload force should not exceed more than 30% of the piezoelectric actuator blocking force. Therefore, the maximum Von-Mises stress of the clamp and feeder sets under the preload are 163 and 44.9 MPa, respectively.

Figure 10 shows the distribution of Von-Mises stress resulted from applying the maximum voltage to the

piezoelectric actuator (in addition to the preload) in the clamp mode. As seen in the figure, the maximum stress is approximately 275 MPa which occurs in the surrounding areas of the clamp grooves and is far from the yield stress of the heat treated steel (1700 MPa).

Figure 11 shows the Von Mises stress distribution of piezomotor in the feeder mode. By taking the pre-load stress of the actuators into account, the maximum stress is about 121 MPa induced in the interfacing ridges of the springs because of the reduced efficient cross-section. As similar to the clamp actuator, the feeder structure also has an excellent margin of safety in comparison with the yield stress of the material.

3.3 Step Size Test

Figure 12 demonstrates the step size of the piezomotor versus the voltage in the range of 7 to 20 V. The points of the plot indicate the experimental data, while the fitted curve displays a rough estimation of the behavior for this system. As is apparent from the figure, the fitted curve demonstrates the linear behavior of the system. The least and the most step response of the piezomotor corresponds to 7 and 20 V are 1.09 and 3.25 μm , respectively. Also, the resolution of the piezomotor corresponds to the 0.5 V is 81 nm. This parameter is adjustable by changing the applied voltage. Since the behavior of the piezo stack actuators are almost linear under the operating voltage, this analysis shows the linear behavior of the proposed piezomotor.

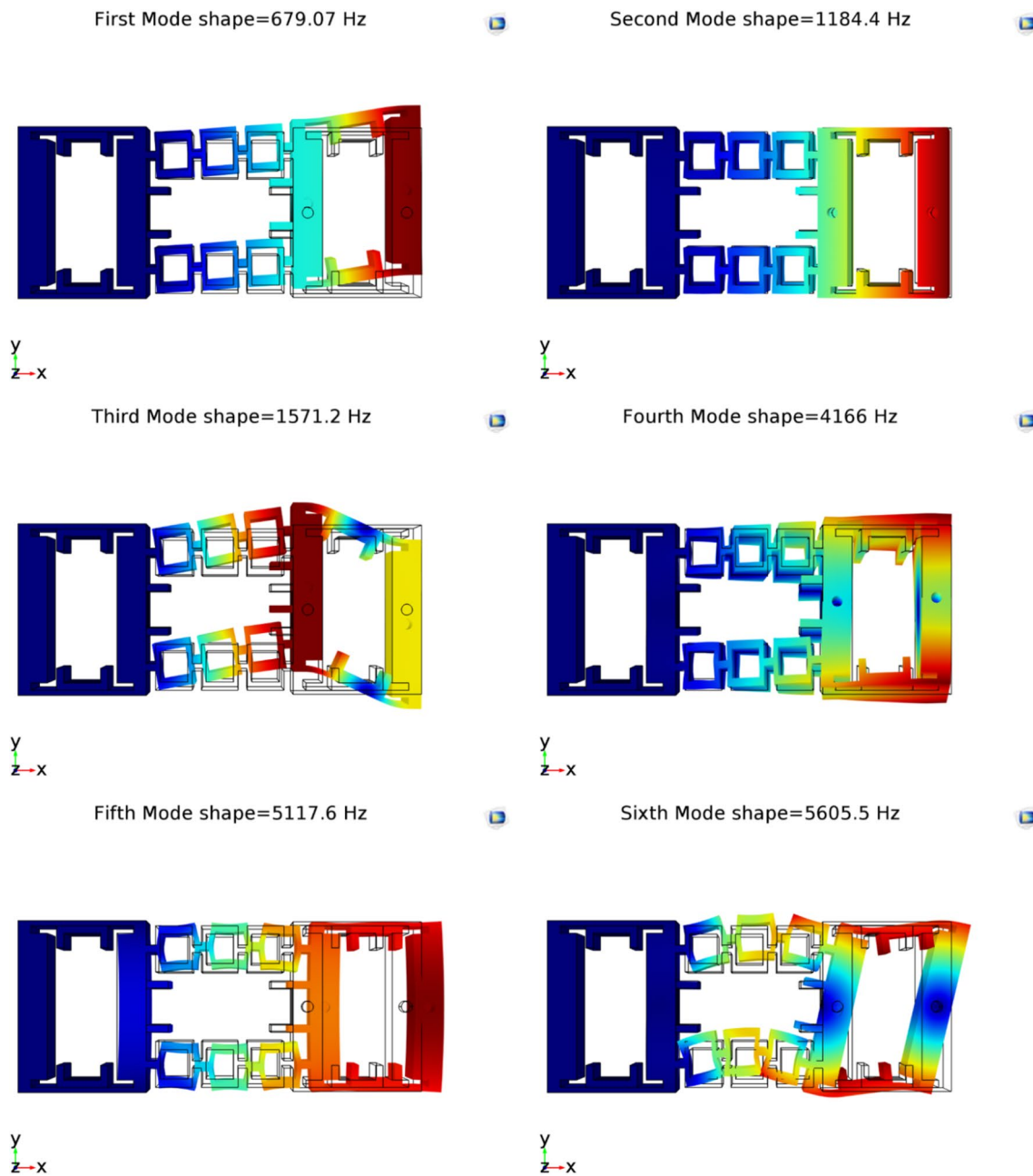


Fig. 9 First six resonance modes of the one-axis piezomotor

3.4 Speed Response

The axial speed of a piezomotor determines by two main factors which are applied voltage frequency and amplitude. Since the maximum operating frequency is always less than the resonant mode of the system, this section investigates the axial speed as well as the operating frequency of the piezomotor. Figure 13 demonstrates the speed-frequency characteristics of the proposed piezomotor. By increasing the frequency, the speed grows linearly, which shows the

linear behavior of this motor in the frequencies up to 150 Hz. The maximum operating frequency is equal to 150 Hz which creates the maximum speed of 1.075 mm/s. If the frequency exceeds from 150 Hz, the speed drops significantly and eventually the motor stops at the frequency of 300 Hz. As it studied earlier on the Sect. 3.1, this sudden degradation is because of approaching to the resonant mode of the system. In summary, the maximum speed for this piezomotor is 1.075 mm/s which happens at the operating frequency of 150 Hz.

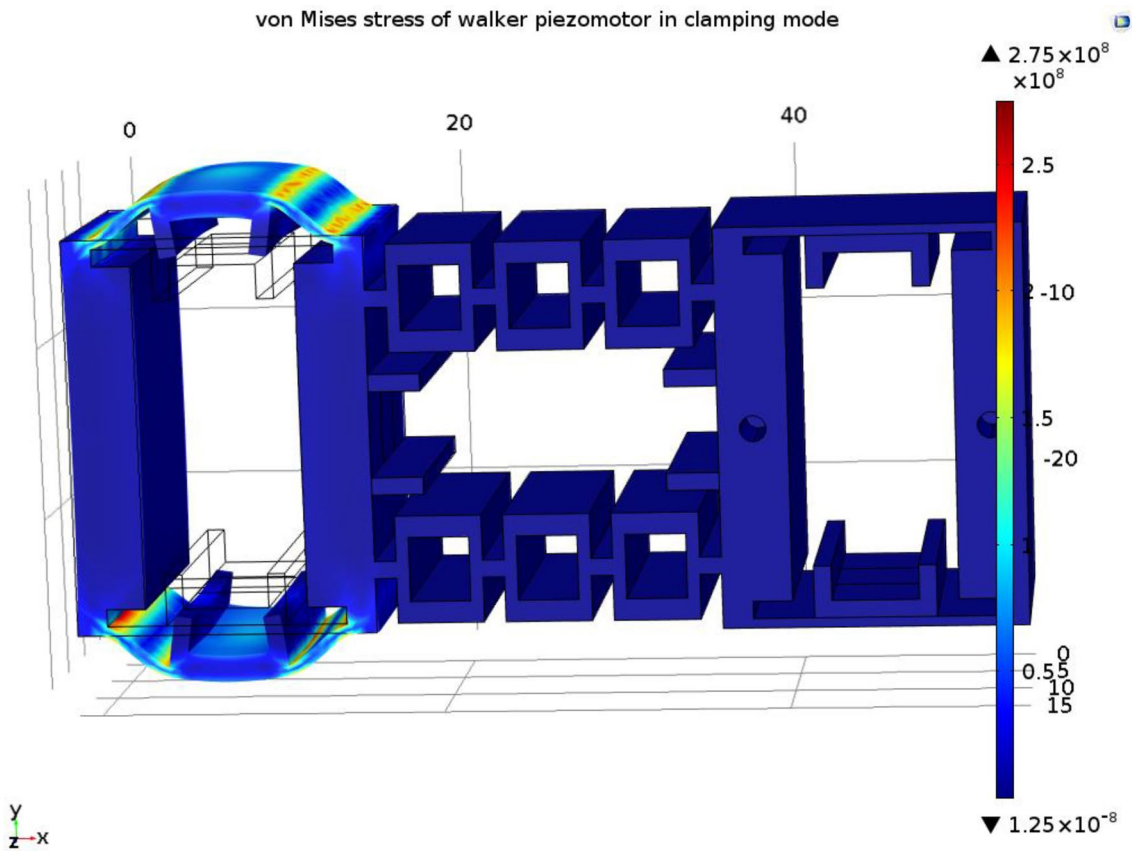


Fig. 10 Von Mises stress distribution in the clamp mode

4 Conclusion

In this research, a high-speed, high-stroke and low-cost one-axis inchworm walker piezomotor was designed, manufactured and characterized. By using the Finite Element Analysis (FEA) method, the effects of the geometrical parameters on the axial stiffness were computed. By a proper selection of geometric parameters, the stiffness of clamps and feeder were determined as 11.08 N/ μm and 46.45 N/ μm , respectively. FEA analysis also was carried out to realize the resonance modes and Von Mises stress distribution in the piezomotor structure. The primary

resonance modes of the piezomotor occur at first mode with a frequency of 579.07 Hz, and the fifth mode with a frequency of 5117.6 Hz, which are high enough to avoid resonance disturbance under the operation conditions. Also, the maximum Von Mises stress is 275 MPa which provides a high margin of safety for the system structure. Finally, the experimental tests were implemented to realize the resolution, speed, and the maximum operating frequency of the piezomotor as 81 nm, 1.075 mm/s and 150 Hz, respectively. The movement step size and resolution of the proposed piezomotor can be altered by adjusting the driving voltage.

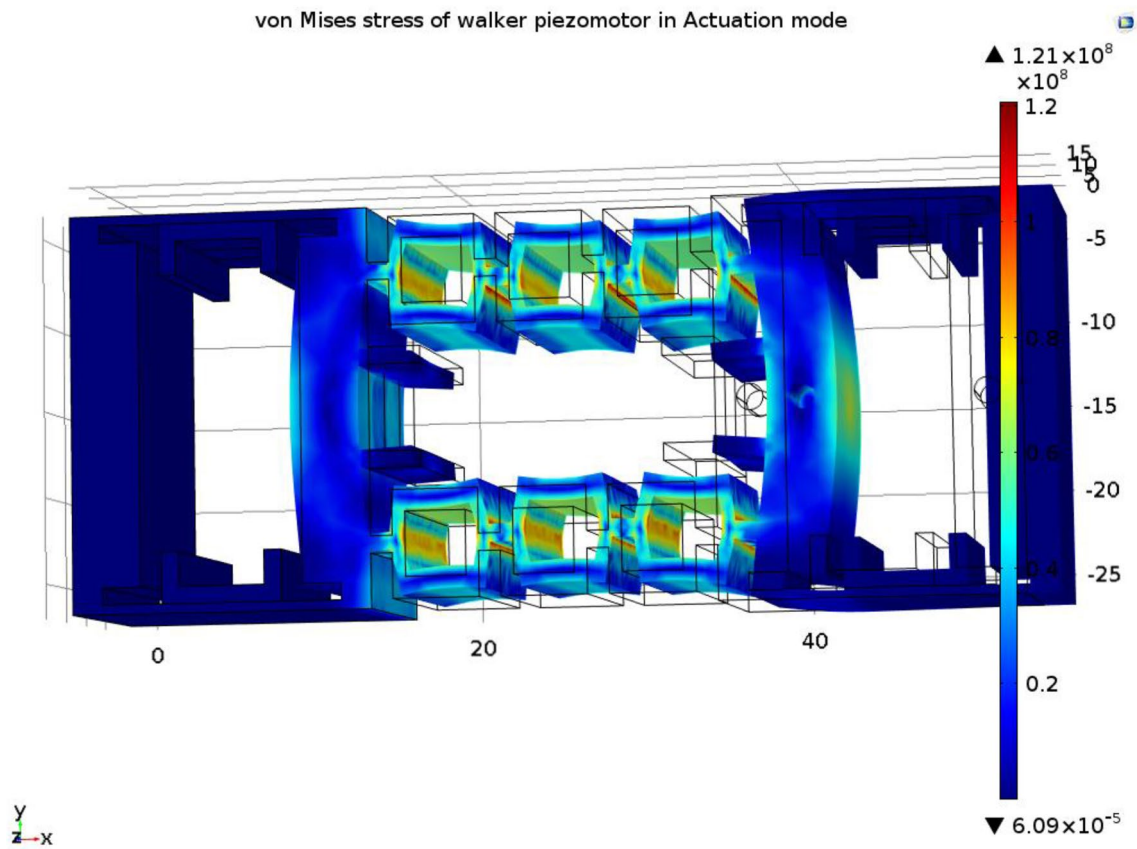


Fig. 11 Von Mises stress distribution in the feeder mode

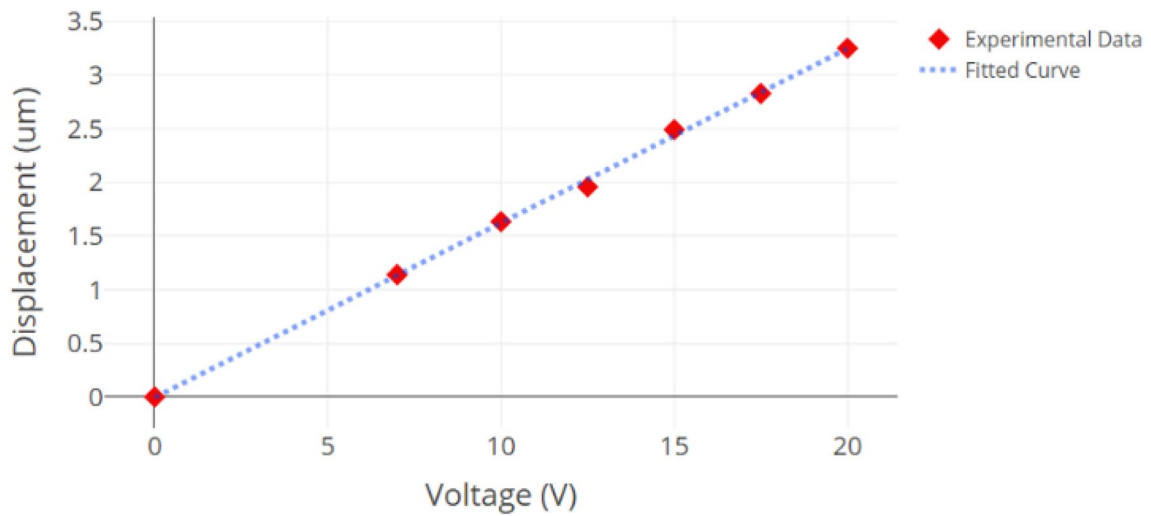


Fig. 12 Step size of the piezomotor versus applied voltage

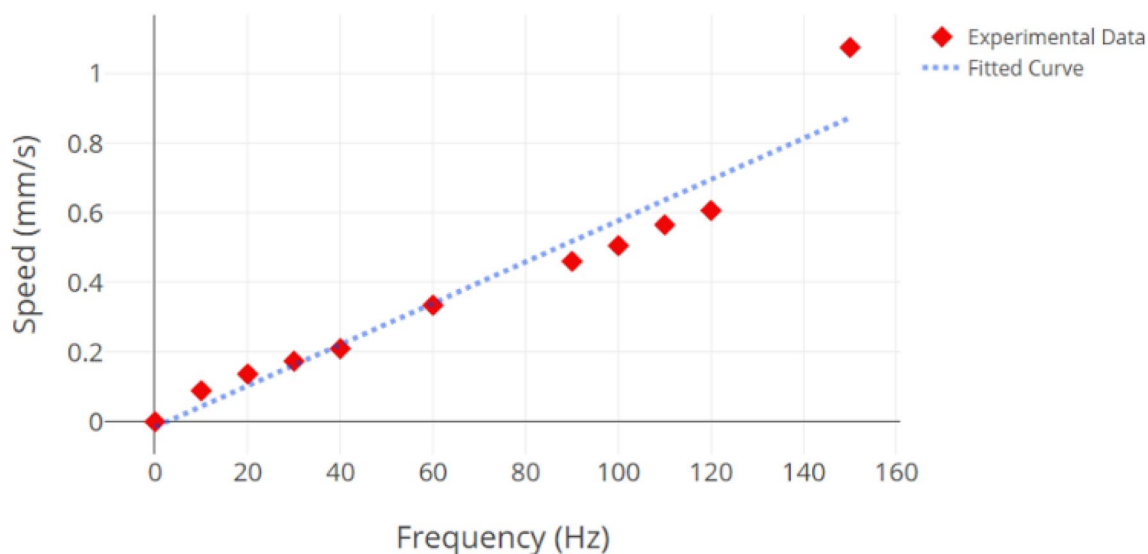


Fig. 13 The speed of the piezomotor versus frequency of the applied voltage

References

- Cao Y, Chen XB (2015) A survey of modeling and control issues for piezo-electric actuators. *J Dyn Syst Meas Contr* 15:014001
- Fleming AJ, Leang KK (2014) Design, modeling and control of nanopositioning systems. Springer International Publishing, Switzerland
- Fujimoto T (1988) Linear motor driving device. US Patent 4,736,131
- Galante T, Frank J, Bernard J, Chen W, Lesieutre GA, Koopmann GH (1999) Design, modeling, and performance of a high force piezoelectric inchworm motor. *J Intell Mater Syst Struct* 10:962–972
- Gao P, Tan H, Yuan Z (2000) The design and characterization of a piezo-driven ultra-precision stepping positioner. *Meas Sci Technol* 11:15
- Ma L, Xiao J, Zhou S, and Sun L (2015) A piezoelectric inchworm actuator of linear type using symmetrical lever amplification. In: Proceedings of the Institution of Mechanical Engineers Part N: Journal of Nanoengineering and Nanosystems. Vol 229, pp 172–179
- Pan JT (2000) Linear Actuator. US Patent 6,104,125,15
- Peng Y, Gu X, Wang J, Yu H (2015) A review of long range piezoelectric motors using frequency leveraged method. *Sens Actuators, A* 235:240–255
- Powers GD, Xu Q, Fasick JC, Smith JA (2003) Nanometer resolution actuator with multimillimeter range and power-off hold. *Smart Struct Mater Ind Commer* 5054:108–117
- Roberts D (1999) Development of a linear piezoelectric motor based on the inchworm model. *Smart Struct Mater* 3668:705–716
- Ru C, Liu X, Sun Y (2016) Nanopositioning technologies. Springer, Berlin
- Shafik A, Mrad RB (2016) Piezoelectric motor technology: a review nanopositioning technologies. Springer, Cham, pp 33–59
- Spanner K (2006) Survey of the various operating principles of ultrasonic piezomotors. In: Proceedings of the 10th International Conference on New Actuators
- Tahmasebipour G, Ahmadi V, Abdullah A, Hojjat Y (2009) Fabrication of STM W nanotip by electrochemical etching method. *Int J Nanosci* 3:305–310
- Tahmasebipour G, Ahmadi V, Abdullah A (2010) Optimization of electrochemical etching parameters in FIM/STM tungsten nanotip fabrication. *J Sci Islam Repub Iran* 21:75–83
- Tahmasebipour M, Tahmasebipour Y, Shabani AA, Boujari M (2017) Effect of micro wire-EDM process parameters on recast layer in the molybdenum micromachining. *J Adv Design Manuf Technol* 10(1):101
- Tahmasebipour M, Tahmasebipour Y, Vafaie A (2019) Micro wire electrical discharge machining of the mems structures with optimized dimensional deviation. *J Adv Design Manuf Technol* 12(2):103
- Tahmasebipour G, Tahmasebipour Y, Ghoreishi M (2011) Computational fluid dynamic simulation of the nanoelectrical discharge machining process. *NANO* 6:561–568
- Tahmasebipour Y, Ghoreishi M, Tahmasebipour M (2014) Finite-volume heat transfer model of the nano electrical discharge machining process. *J Nanoelectron Optoelectron* 9:605–611
- Galutva GV, Ryazantsev AI, Presnyakov GS, Modestov JK (1972) Device for Precision Displacement of a Solid Body US Patent 3,684,904
- Tenzer PE, Mrad RB (2004) A systematic procedure for the design of piezoelectric inchworm precision positioners. *IEEE/ASME Trans Mechatron* 9:427–435
- Vijaya MS (2016) Piezoelectric materials and devices: applications in engineering and medical sciences. CRC Press, Boca Raton
- Yong YK, Moheimani SR, Kenton BJ, Leang KK (2012) Invited review article: high-speed flexure-guided nanopositioning: Mechanical design and control issues. *Rev Sci Instrum* 83:121101
- Zhang B, Zhu Z (1997) Developing a linear piezomotor with nanometer resolution and high stiffness. *IEEE/ASME Trans Mechatron* 2:22–29
- Zhang B, Zhu Z, Fu WE, Wang J (1997) A linear piezomotor of high stiffness and nanometer resolution. *CIRP Ann* 46:305–308